

XMM-NuSTAR monitoring of GX 339-4 during its transition back to the hard state

P.O. Petrucci, M. Clavel, S. Corbel, S. Chakravorty, J. Rodriguez, F. Ursini,
J. Ferreira, R. Belmont, J. Malzac, G. Henri, M. Coriat, S. Drappeau, J. Tomsick

The Campaign

The XMM-Newton/NuSTAR monitoring started on August 28, 2015 and ended on September 30, 2015. The goal of the campaign was to follow the transition back to the hard state of GX 339-4 at the end of its outburst, when the source goes back to quiescence (see Fig. 1 and the observation logs in Tab. 1 and 2).

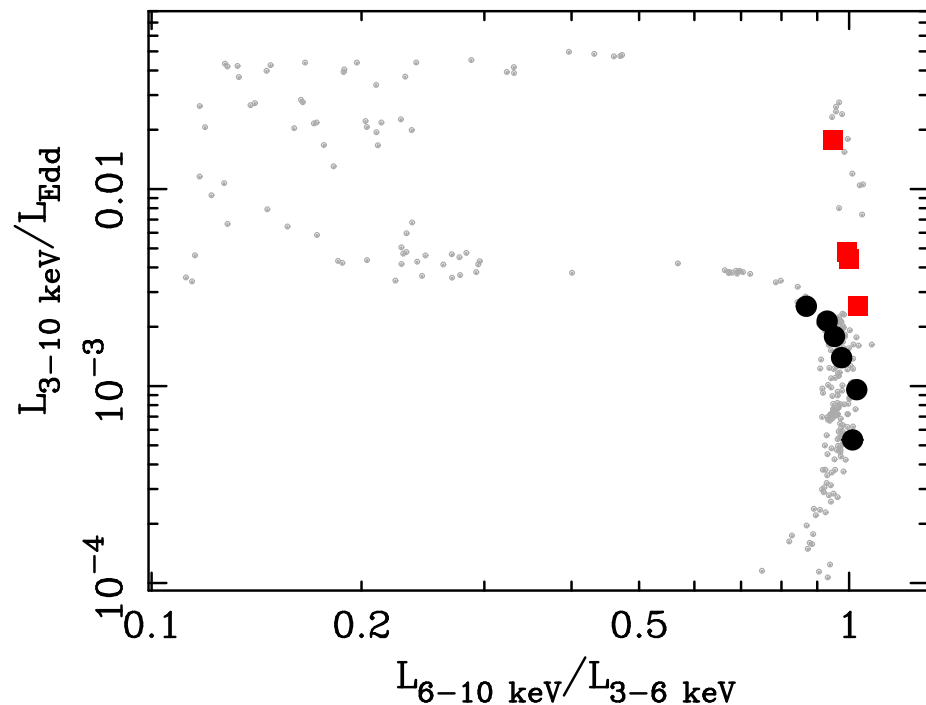


Figure 1: The HID of GX339-4. The black dots refer to the XMM observation analysed in this poster. The red squares are the archival XMM observations of GX 339-4 performed during the 2009 and 2004 outbursts. For reference, the gray dots show the pattern of a full outburst observed by RXTE in 2009. From De Marco et al. (2017)

Observation Logs

XMM observation log						
Obs ID	Date (MJD)	Date	Exposure Total/Net (ks)	Mean count rate tot/0.5-2 keV/2-10 keV (cts/s)		Obs. mode
Obs 1	0760646201	57262.74	28 Aug. 2015	18.9/9.4	236/152/76	Timing
Obs 2	0760646301	57267.62	02 Sep. 2015	18.1/15.7	158/94/60	Timing
Obs 3	0760646401	57272.70	07 Sep. 2015	22.6/20.2	124/72/48	Timing
Obs 4	0760646501	57277.69	12 Sep. 2015	21.0/18.6	92/51/38	Timing
Obs 5	0760646601	57282.68	17 Sep. 2015	52.4/36.5*	53/29/21	Small window
Obs 6	0760646701	57295.09	30 Sep. 2015	48.1/33.4*	27/14/12	Small window

Table 1: Obs ID, date in MJD and calendar format, total and net exposure (after filtering for flaring particle background if any), mean count rate in the 0.5-2 and 2-10 keV range, and observing mode (-30% of deadtime in small window mode).

NuSTAR observation log						
Obs ID	Date (MJD)	Date	Exposure Net (ks)	Mean count rate ¹ 3-10 keV/20-70 keV (cts/s)		
Obs 1	80102011002	57262.54	28 Aug. 2015	21.6	12.3/1.2	
Obs 2	80102011004	57267.53	02 Sep. 2015	18.3	10.4/ 1.2	
Obs 3	80102011006	57272.62	07 Sep. 2015	19.9	8.7/ 1.1	
Obs 4	80102011008	57277.66	12 Sep. 2015	21.5	6.8/ 0.8	
Obs 5	80102011010	57272.62	17 Sep. 2015	38.5	4.8/ 0.6	
Obs 6	80102011012	57295.05	30 Sep. 2015	19.9	2.5/ 0.3	

Table 2: Obs ID, date in MJD and calendar format, net exposure, mean count rate in the 3-10 and 20-70 keV range. These count rates are the algebraic mean of the FPMA and FPMB,

Data Treatment

XMM-Newton: Timing Mode

- ▶ Run epproc
- ▶ Filter the EPIC event list for flaring particle background.
- ▶ No pile-up
- ▶ The source is too bright and prevent the extraction of clean background spectra. No background is used for this mode.

XMM-Newton: Small window

- ▶ Run epproc
- ▶ Filter the EPIC event lists for flaring particle background.
- ▶ Pile-up lower than 4%. No pile-up correction is applied.
- ▶ Filter the OoT events
- ▶ Pollution from dust scattering halo is not important
- ▶ The source is too bright and prevent the extraction of clean background spectra. No background is used.

NuSTAR

- ▶ We reduced the NuSTAR data using NUSTARDAS v.1.7.0 which is part of HEASOFT 6.20, setting SAAMODE=strict and TENTACLE=YES.
- ▶ For each observation the source and background spectra were extracted from circular regions of 100 and 135-arcsec radii, respectively.

XMM vs NuSTAR

- ▶ XMM and NuSTAR do not agree with each other in the 3-10 keV range
- ▶ Fitting with a power law gives a harder photon index ($\Delta\Gamma > 0.1$) in XMM with respect to NuSTAR (see Tab. 3 and Fig. 3)

Light Curves

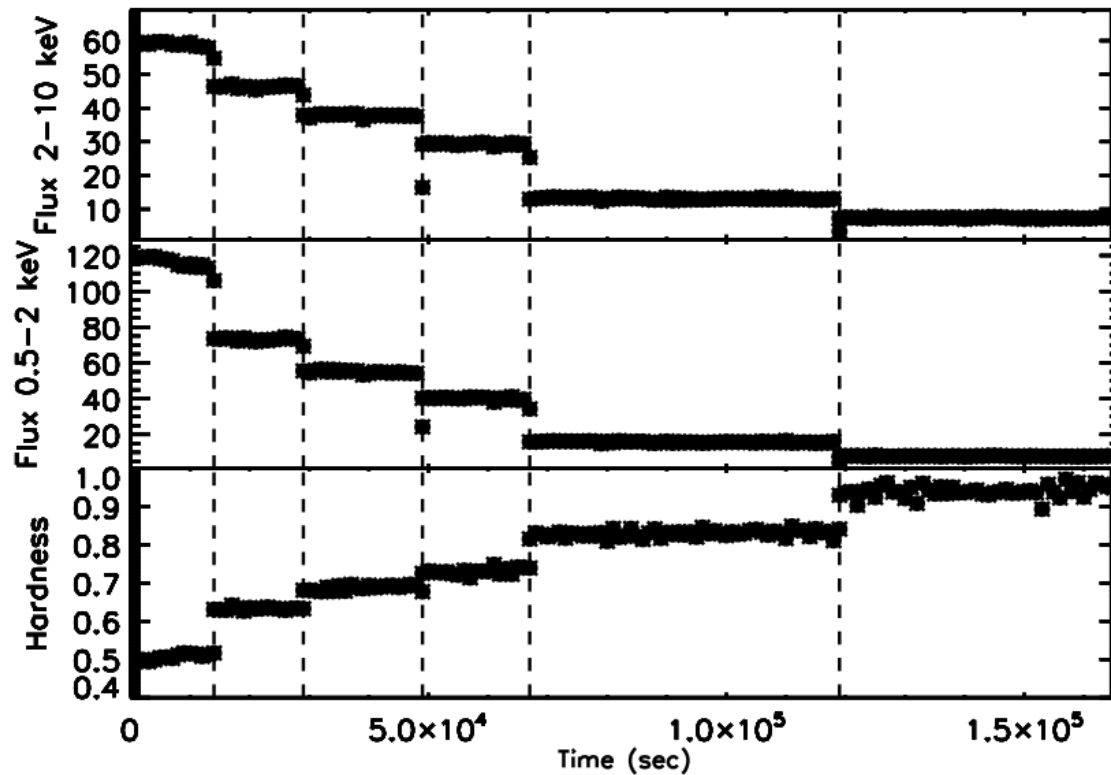


Figure 2: 2-10 keV (top) and 0.5-2 keV (middle) light curves and corresponding hardness ratio for the 6 XMM observations put side by side. The binning is 1ks.

XMM vs NuSTAR

Obs	tied Γ	untied Γ
1	1.78 ± 0.01 $\chi^2/\text{dof}=375/127$	$\Gamma_{XMM}=1.74 \pm 0.02$ $\Gamma_{NuSTAR}=1.85 \pm 0.01$ $\chi^2/\text{dof}=288/126$
2	1.65 ± 0.01 $\chi^2/\text{dof}=380/128$	$\Gamma_{XMM}=1.62 \pm 0.01$ $\Gamma_{NuSTAR}=1.75 \pm 0.02$ $\chi^2/\text{dof}=270/127$
3	1.60 ± 0.01 $\chi^2/\text{dof}=275/114$	$\Gamma_{XMM}=1.58 \pm 0.01$ $\Gamma_{NuSTAR}=1.70 \pm 0.02$ $\chi^2/\text{dof}=185/111$
4	1.54 ± 0.01 $\chi^2/\text{dof}=203/103$	$\Gamma_{XMM}=1.51 \pm 0.01$ $\Gamma_{NuSTAR}=1.65 \pm 0.02$ $\chi^2/\text{dof}=116/101$
5	1.61 ± 0.01 $\chi^2/\text{dof}=290/120$	$\Gamma_{XMM}=1.66 \pm 0.01$ $\Gamma_{NuSTAR}=1.62 \pm 0.02$ $\chi^2/\text{dof}=174/118$
6	1.61 ± 0.01 $\chi^2/\text{dof}=228/96$	$\Gamma_{XMM}=1.65 \pm 0.01$ $\Gamma_{NuSTAR}=1.63 \pm 0.03$ $\chi^2/\text{dof}=146/94$

Table 3: Photon index best fits values obtained by fitting simultaneously the XMM/PN data between 3 and 10 keV and the NuSTAR one between 4.5 and 10 keV, ignoring the 5 to 8 keV band, and tying (left) or untying (right) the photon index and power law normalisation between the two data sets.

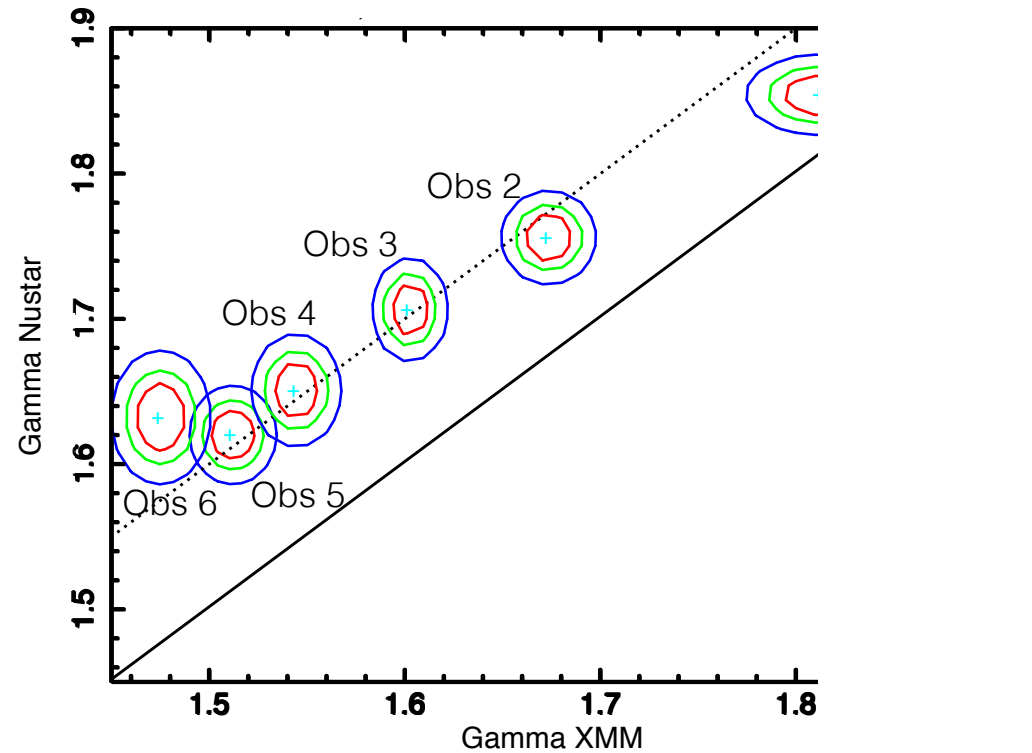


Figure 3: Comparison, for all the observations of the campaign, of the best fit power law photon index of NuSTAR (4.5-10 keV) and XMM/PN (3-10 keV), when the energy range 5-8 keV is ignored (we use the const \times tbabs \times pow model, N_H being fixed to $6 \times 10^{21} \text{cm}^{-2}$). The solid and dotted lines corresponds to $y=x$ and $y=x+0.1$ respectively.

Iron line complex

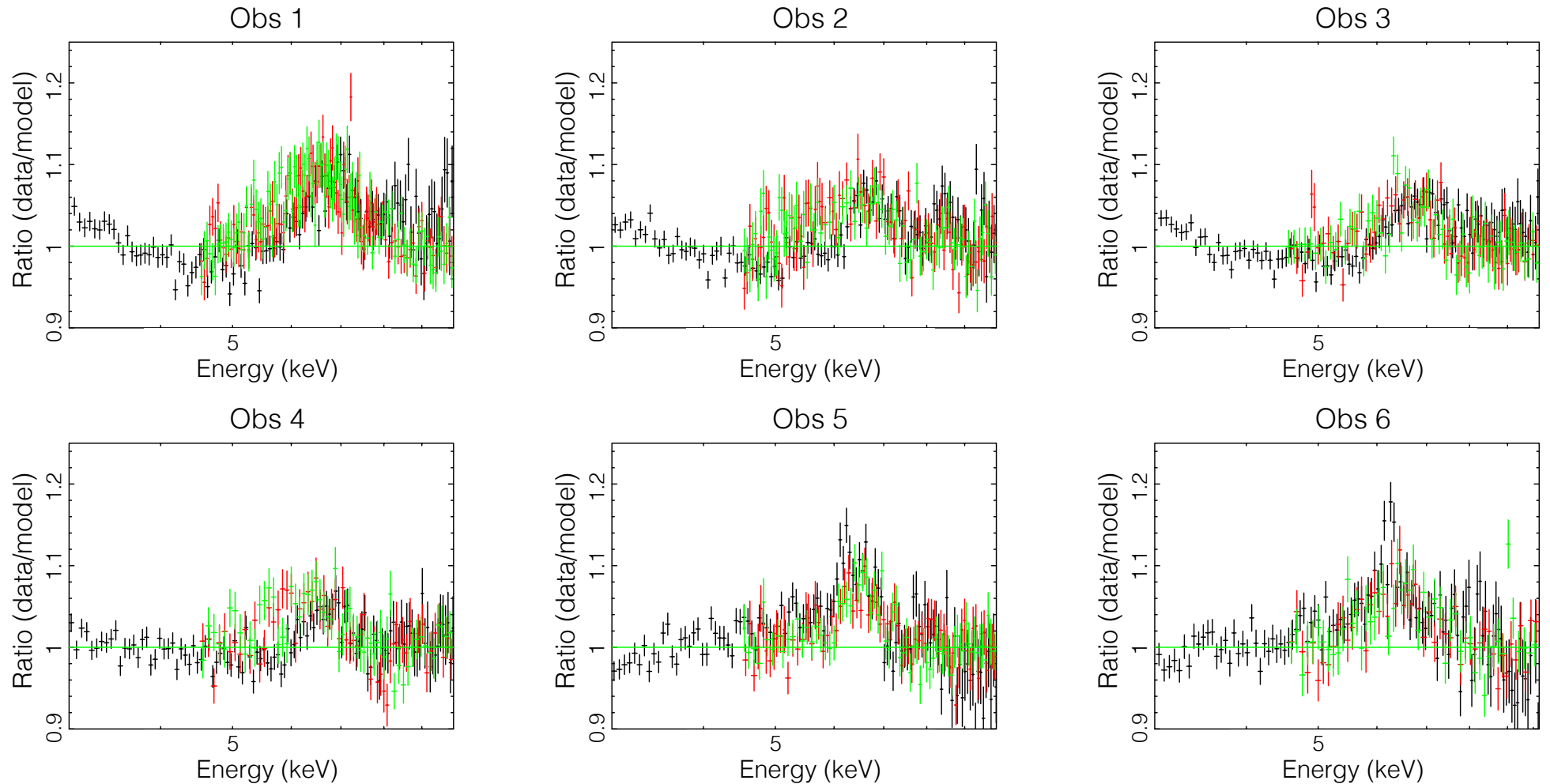


Figure 4: Ratio data/model when fitting with a power law ignoring the 5-8 keV energy range. An excess in the 5-8 keV range is always visible signature of the presence of iron line emission. Fits with a gaussian for the line are reported in Tab. 4.

Obs	Γ_{XMM}	Γ_{NuSTAR}	E_{Fe} (keV)	σ_{Fe} (keV)	F_{Fe} ($10^{-3}\text{cm}^{-2}\text{s}^{-1}$)	EW (eV)	$F_{3-10keV}$ ($10^{-10}\text{erg cm}^{-2}\text{s}^{-1}$)	χ^2/dof	$\Delta\chi^2$
Obs 1	1.74±0.01	1.86±0.01	6.66±0.05	0.63±0.07	7.6±1.0	120±20	5.1	520/317	489
Obs 2	1.63±0.01	1.77±0.01	6.67±0.06	0.43±0.10	3.2±0.5	60±10	4.2	466/268	201
Obs 3	1.58±0.01	1.72±0.02	6.77±0.07	0.50±0.08	3.5±0.6	80±20	3.5	341/233	209
Obs 4	1.52±0.01	1.67±0.02	6.58±0.08	0.40±0.07	1.9±0.4	55±10	2.8	271/225	139
Obs 5	1.65±0.01	1.61±0.02	6.36±0.10	0.44±0.15	2.4±0.4	100±20	1.8	348/244	316
Obs 6	1.66±0.01	1.59±0.02	6.13±0.10	0.81±0.15	2.5±0.5	180±30	1.0	268/207	274

Table 4: Best fit parameter values using the XSPEC model $\text{const} \times \text{tbabs} \times (\text{pow} + \text{gauss})$ in the 3-10 keV range, N_{H} being fixed to $0.6 \cdot 10^{22} \text{ cm}^2$. The last column gives the decrease in χ^2 due to the addition of a gaussian (with 3 more dof).

Broad band continuum

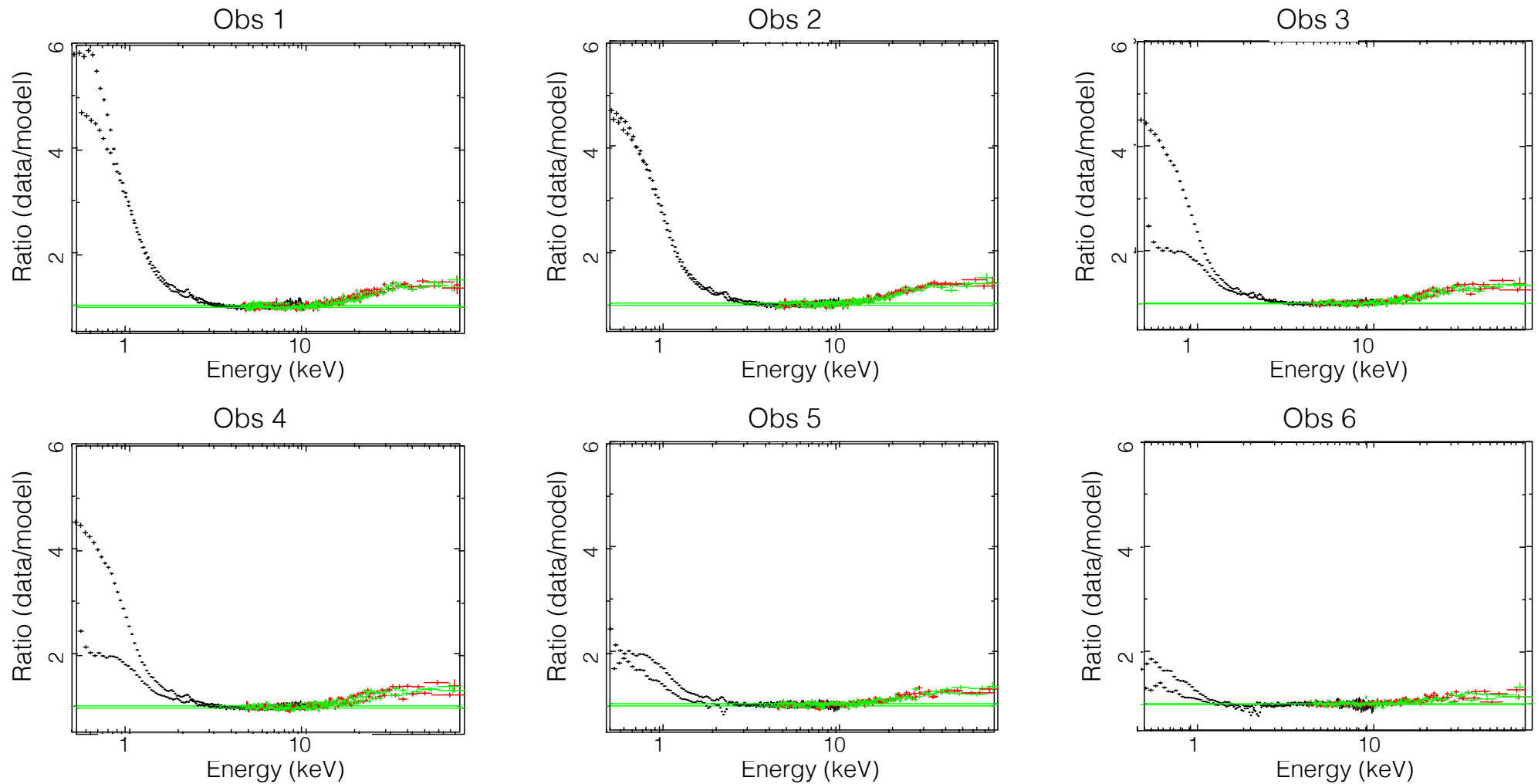


Figure 5: Ratio XMM/NuSTAR data/model when extrapolating the 3-10 keV power law fit down to 0.5 keV and up to 79 keV. A soft X-ray excess and a high energy bump are clearly visible, both decreasing with time (see also Fig. 6).

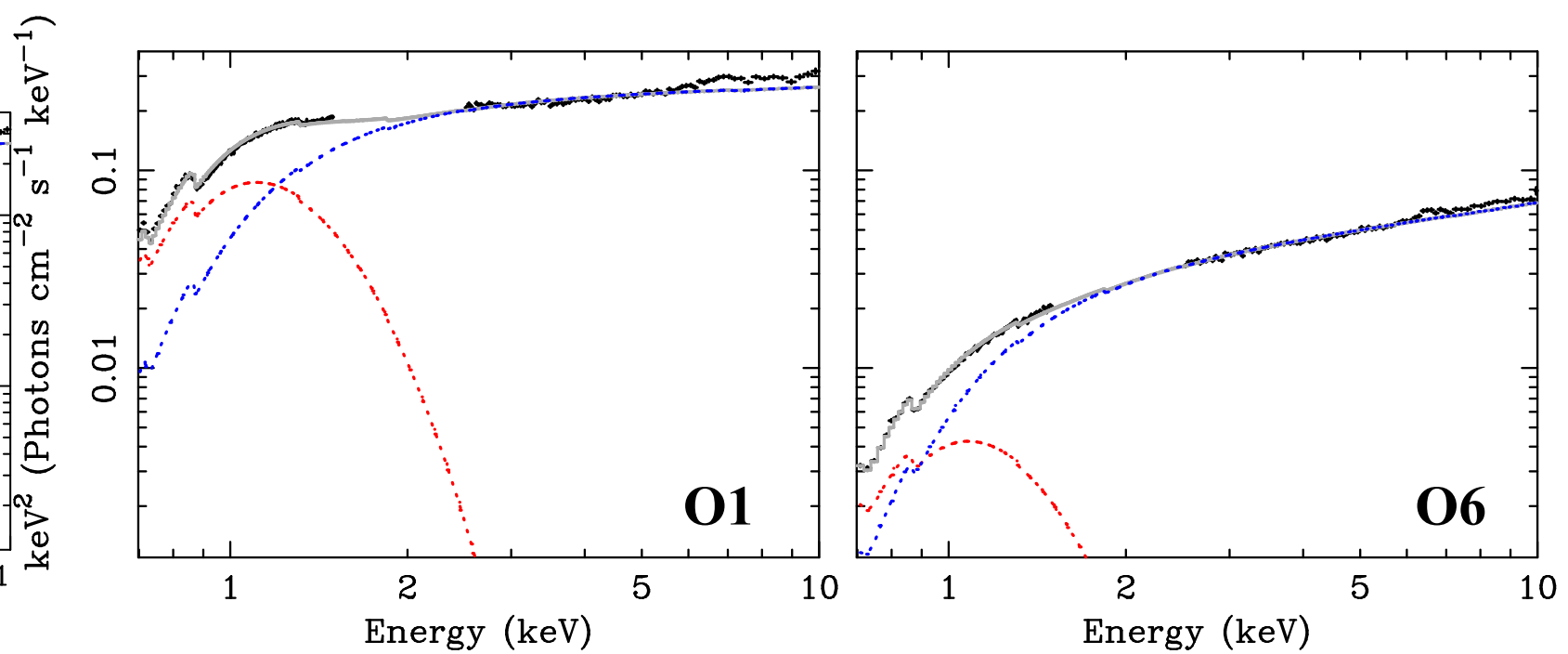


Figure 6: The plots show the EPIC pn unfolded spectra of the first (O1, left panel) and the last observation (O6, right panel) of the monitoring. Overplotted is the best-fit model (solid gray curve) and the single components of the model (i.e. diskbb, red dotted curve, and nthComp, blue dotted curve).

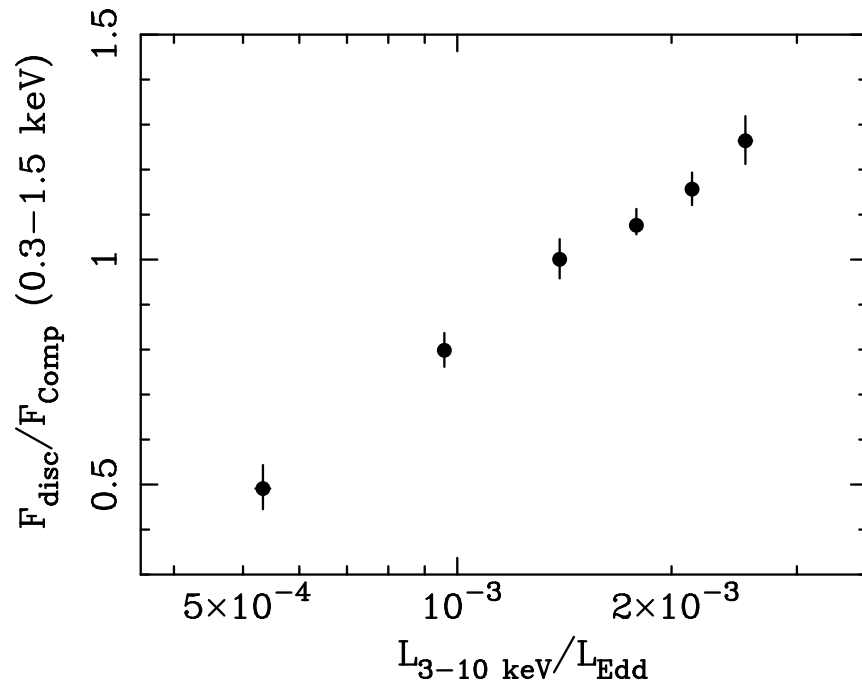


Figure 7: Disc-to-power law flux ratios (in the energy range 0.3-1.5 keV) as a function of 3-10 keV Eddington-scaled luminosity.

Spectral analysis: first results

- ▶ During the transition, the source decreases in flux (Fig. 1 and 2) and its spectrum hardens (Tab. 3 and Fig. 3)
- ▶ Problem of intercalibration between the XMM/PN and NuSTAR data, the XMM/PN data being harder than the NuSTAR one ($\Delta\Gamma > 0.1$, Tab. 3 and Fig. 3)
- ▶ An iron line is always present. When fitted with a gaussian it is clearly broad (see Fig. 4, Table 4).
- ▶ A strong soft X-ray excess as well as a reflection bump are also present all along the campaign, their importance however decreasing from OBS 1 to OBS 6 (see Fig. 5, 6 and 7)

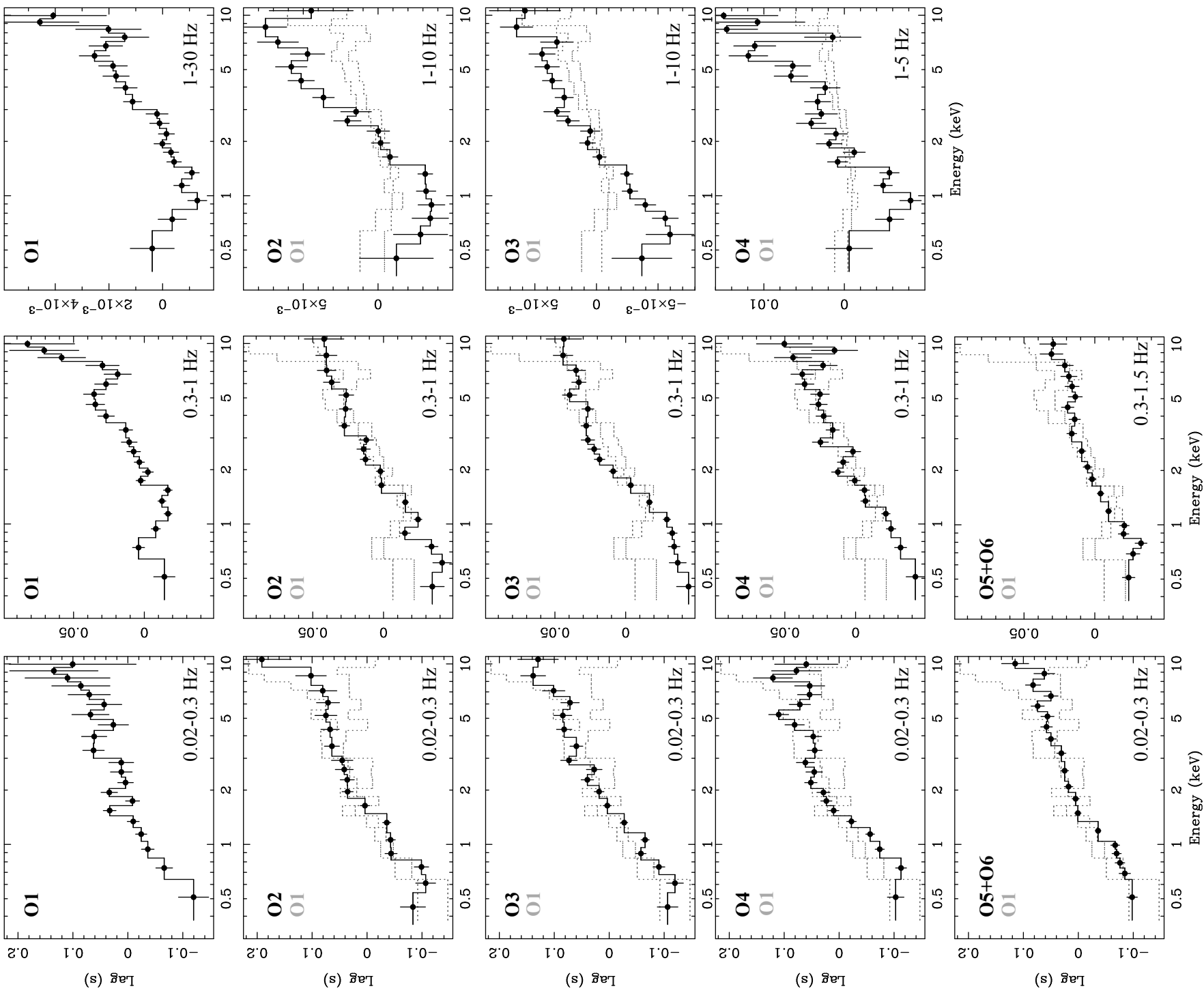


Figure 8: Lag-energy spectra of the different observations (Obs 1 to Obs 6, from top to bottom) in the low, medium, and high frequency range (from left to right), as computed between a broad reference band (0.5-10 keV) and adjacent small energy bins. To facilitate comparison among the spectra of the different observations, for each frequency range we overplot the contours (gray dashed lines) of the lag-energy spectrum of Obs 1. From De Marco et al. (2017).

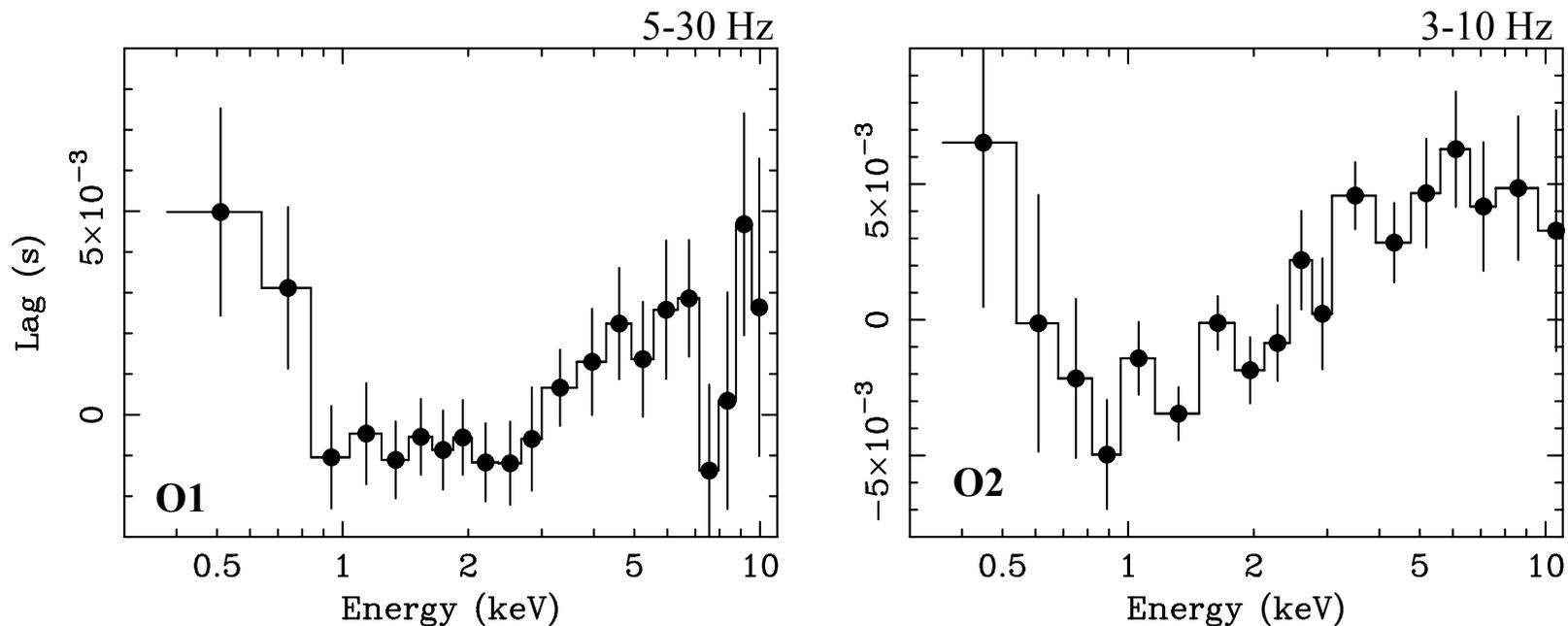


Figure 9: Lag-energy spectra of observations O1 (left panel) and O2 (right panel) restricted to the very-high frequency range, which extends up to 30 Hz for O1 and up to 10 Hz for O2.

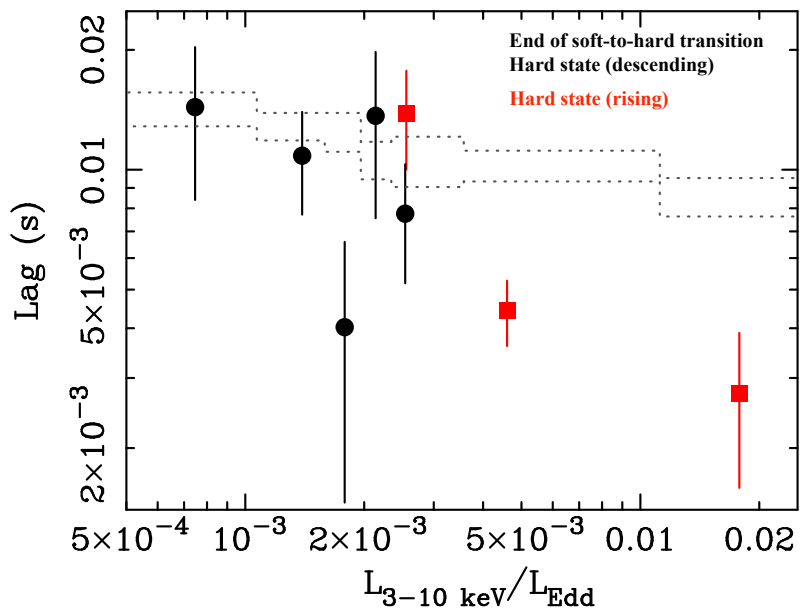


Figure 9: The reverberation lag amplitude as a function of 3-10 keV Eddington-scaled luminosity. The black dots refer to the estimates obtained in this campaign. The red squares are estimates obtained in De Marco et al. (2015) from archival XMM observations during the 2009 and the 2004 outburst (see Fig. 1). The gray dotted lines represent the 1σ contours showing the expected trend of observed lag amplitude as a function of luminosity induced by variations of the relative fraction of thermally reprocessed flux to the direct variable continuum, and assuming a constant value for the intrinsic reverberation lag.

Timing Analysis

De Marco et al. (2017)

- ▶ A soft X-ray lag ascribable to disc thermal reverberation is observed during all the observations when frequencies ~ 1 Hz are sampled (see Fig. 8).
- ▶ We observe a net decrease of lag amplitude (by a factor ~ 5) as a function of luminosity.
- ▶ The observed dependence of reverberation lag amplitude on luminosity could be related to variations of the geometry of the inner accretion flow. In particular, an inner disc truncation radius approaching the ISCO as the luminosity increases at the beginning of the outburst and receding as the luminosity decreases at the end of the outburst is in agreement with our results.

Data Analysis in Progress

To be done:

- ▶ Use of more realistic comptonisation model for the continuum
- ▶ Use of more realistic reflection models
- ▶ Test for relativistically blurred iron line
- ▶ Test of different soft X-ray excess models